2019-04-23

# Dynamic FOV visible light communications receiver for dense optical networks

**Accepted Article** – In I. Abdalla, M. B. Rahaim, and T.D.C., Little, "Dynamic FOV Visible Light Communications Receiver for Dense Optical Networks (Invited Paper)," *IET Communications*, Vol. 3, No. 7. April 2019. https://doi.org/10.1049/iet-com.2018.5784.

# Dynamic FOV Visible Light Communications Receiver for Dense Optical Networks (Invited Paper)

I. Abdalla,[1] M. B. Rahaim,[2] and T.D.C. Little[1]
[1]Department of Electrical and Computer Engineering
Boston University, 8 Saint Mary's St., Boston, MA 02215 USA
[2]Engineering Department,
University of Massachusetts at Boston, Boston, MA USA

**Abstract:** This paper explores how the Field of View (FOV) of a Visible Light Communications (VLC) receiver can be manipulated to realize the best Signal to Noise Ratio (SNR) while supporting device mobility and optimal access point (AP) selection. We propose a Dynamic FOV receiver (D-FOV) that changes its aperture according to receiver velocity, location, and device orientation. The D-FOV technique is evaluated through modeling, analysis, and experimentation in an indoor environment comprised of 15 VLC access points (APs). The proposed approach is also realized as an algorithm that is studied through analysis and simulation.

Results of the study indicate the efficacy of the approach including a 3X increase in predicted SNR over static FOV approaches based on measured Received Signal Strength (RSS) in the testbed. Additionally, the collected data reveal that D-FOV increases effectiveness in the presence of noise. Finally, we describe the tradeoffs among the number of VLC sources, FOV, user device velocity, and SNR as a performance metric.

**Keywords:** Visible Light Communications, Field of View, Optical Receiver, Device Mobility, RSS, SNR.

 This work is supported in part by the Engineering Research Centers Program of the National Science Foundation under NSF Cooperative Agreement No. EEC-0812056 and by NSF No. CNS-1617924. Any opinions, findings, and conclusions or recommendations expressed in this material are those of the author(s) and do not necessarily reflect the views of the National Science Foundation.

# 1 Introduction

Visible Light Communications (VLC) exploits the relatively untapped optical spectrum to provide a new medium on which to allow wireless access [1, 2]. Because light and lighting are ubiquitous, delivering data from lights is an ideal match for indoor spaces. Light is also highly directional and can be shaped [3], for example, spot lights which direct light onto work surfaces such as desks or conference tables. This directionality can also be exploited to create very small cells each with high Signal to Noise Ratio (SNR) [4].

VLC is also commercially available with products that are deployable for point-to-point and point-to-multipoint scenarios [5]. VLC has many advantages, including providing a complementary medium and the possibility of high spatial reuse [4]. However, early VLC products concentrate on delivering data from a single access point (AP) to one or more static receivers. Challenges in user device mobility, integration with RF systems, and design principles for multiple AP systems are just beginning to receive attention.

Many variables affect received SNR and come into play in system design such as room dimensions, AP placement, AP separation, and illumination pattern [6, 7]. On the receive side, parameters such as receiver FOV, orientation, velocity, and distance are responsible for SNR variability. In our work we explore the effect of varying the receive-side parameters including FOV in order to maximize SNR in the presence of many VLC APs. In these multi-luminaire-AP systems, the adjacent lights create shot noise and signal interference that also impacts the SNR at a receiver. In this paper, our objective is to reduce noise by eliminating as many non-signal light sources as possible.

Relevant work in the literature considers the impact of orientation on received signal strength including [8] in which the authors study the effects of receiver orientation and location on the performance of a wearable VLC device. The authors analyze their system performance through outage probability and discuss the relationship between receiver orientation and data rates. The impact of both receiver FOV and orientation is also studied in [9]. Here the authors develop a system model and related experiments to characterize an indoor space and establish how FOV impacts the design of handover between APs. These works highlight the importance of studying these parameters in theoretical models and how they affect overall system performance.

Motivated by the aforementioned work, we propose a Dynamic Field of View (D-FOV) receiver that adapts a receiver's FOV according to its orientation, location, and velocity. With the use of D-FOV, a receiver can adjust to changing conditions, finding the optimal configuration. For example, by using a wide FOV to search for and acquire a link and then a narrow FOV to isolate a transmitter to improve link performance. We then formulate an optimization problem as a tool to find the best FOV for the maximum SNR at the receiver, which we use to formulate an algorithm with fast response. We show the performance of this D-FOV technique under test using a testbed facility equipped with 15 VLC APs [10]. The main contributions of this paper are:

- Proposed D-FOV receiver
- Static optimization problem
- Dynamic algorithm
- Simulated/theoretical analysis
- Evaluation through empirical data

The remainder of the paper is organized as follows. Section 2 describes our system model for D-FOV. Section 3 explores our optimization problem formulation and our proposed novel velocity algorithm. Section 4 shows our simulation results. Section 5 discusses the data we measured in our testbed facility. Section 6 concludes the paper.

# 2 System Model

Here we introduce our proposed Dynamic Field of View (D-FOV) technique to increase SNR under different operating conditions. The model for D-FOV is also employed in the design of a D-FOV algorithm to dynamically adapt the receiver aperture using velocity and orientation information.

## 2.1 Channel Model

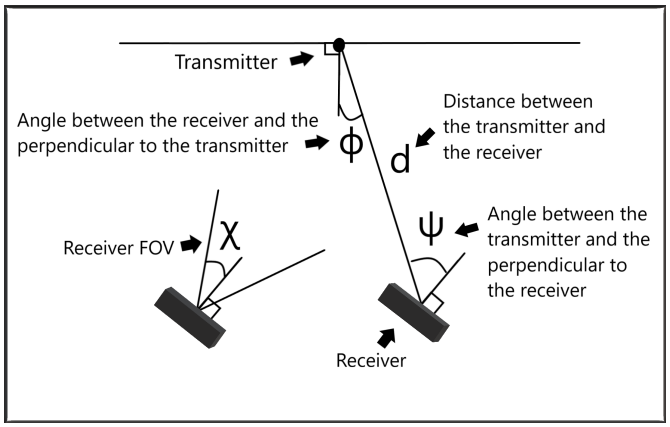


Figure 1: Receiver Device Orientation with Respect to Overhead Access Point (Transmitter)

We consider signal transmission via Intensity Modulation with Direct Detection (IM/DD). The conversion between the electrical and optical domains is considered. We operate in the system's linear range and evaluate the peak-to-peak amplitudes of the received $A_y^{(i)}$ and

transmitted $A_x^{(i)}$ electrical current signals which are related as follows [9]:

$$\frac{A_y^{(i)}}{A_x^{(i)}} = \begin{cases} \frac{C_T C_R (m+1)}{2\pi d_i^2} \cos^m(\phi_i) \cos(\psi_i) & \psi < \chi \\ 0 & otherwise \end{cases} \tag{1}$$

where $C_T$ and $C_R$ are empirically measured proportionality constants that account for the fixed parameters within the system that relate to the transmitter and receiver gains respectively; such as receiver area ($A$), responsivity and optical conversion factor. Meanwhile, $m$ is the Lambertian emission order and we use no filter or optical lens, therefore the lens gain is 1. $\chi$ is the receiver's FOV, $\phi_i$ is the emittance angle, (i.e., the angle between the line from the transmitter to the receiver and the line perpendicular to the $i^{th}$ transmitter), $\psi_i$ is the acceptance angle, (i.e., the angle between the line from the receiver to the $i^{th}$ transmitter and the perpendicular line to the receiver) and $d_i$ is the distance between the $i^{th}$ transmitter and the receiver, as is shown in Fig. 1.

# 3 Optimization Problem and Velocity Algorithm

In this section we formulate the optimization problem. Our objective is to maximize SNR at a receiver under various operating conditions described next.

## 3.1 Optimization Problem

We use commercial LED-based CREE luminaires in our testbed and adopt their characteristics to populate our model. They are rectangular, and we model each one as a grid of $w \times n$ point sources (or elements). For an OOK-modulated signal, the SNR can be modeled as:

$$SNR = \frac{\sigma_s^2}{\sigma_a^2} \tag{2}$$

where $\sigma_s^2$ is the signal variance and $\sigma_a^2$ is the noise current variance. $\sigma_s^2 = A_y^2$ for an OOK-modulated signal, where $A_y$ is the peak-peak electrical current amplitude received in Eq. 1.

While any VLC system has noise contributed by thermal and shot origins, some may be thermal-noise-dominated and others shot-noise-dominated [11]. Our system belongs to the second category, for example, the thermal noise caused by our receiver is around $1.26\mu V$ rms [12] while shot noise is $7.18mV$ rms at a $FOV = 20°$.

For a shot-noise-dominated system, the noise current variance $\sigma_a^2$ is modeled as follows [13]: Shot noise is caused by both dark current noise and quantum noise. Dark current noise $\overline{i_d^2}$ is caused by the current flowing in the photodiode independent of the optical signal. $\overline{i_d^2} = 2qI_dB$ where $q$ is the electron charge, $I_d$ is the dark current and $B$ is the receiver

bandwidth. Meanwhile, quantum noise $\overline{i_q^2}$ is due to the discrete nature of the photodetection process.

$$\overline{i_q^2} = 2qBRP_n \tag{3}$$

where $R$ is the receiver responsivity $[Amp/Wt]$ and $P_n$ $[Wt]$ is the average optical noise power incident on the photodiode. $\sigma_a^2 = \overline{i_d^2} + \overline{i_q^2}$.

$RP_n$ is proportional to $A_y$, which we defined in Eq. (1), as it accounts for $R$ in the $C_T C_R$ constant and so we define the Signal to Noise Ratio (SNR) from transmitter $j$ as

$$SNR_j(\chi) = \frac{(\sum_i A_{ji} 1\{\psi_{ij} \leq \chi\})^2}{\sigma_a^2} \tag{4}$$

where $A_{ji}$ is the received electrical amplitude from element $i$ within the source $j$, $\sum_i^{wn} A_{ji}$ is the total electrical amplitude received from source $j$, $wn$ is the number of elements in the luminaire grid and $1\{.\}$ represents the indicator function. In our analysis, we sum the square of the amplitudes of the OOK signals for different elements ignoring the difference in propagation delay, considering it negligible.

Empirically, we get the signal power by measuring the observed voltage. To compare it with the theoratical model, we need to convert it back to current. To relate $\sigma_a^2$ to noise voltage variance $\sigma_n^2$ we use [12]

$$V_{out} = P_{opt} RMG \tag{5}$$

where $V_{out}$ is the output voltage from the photodiode, $P_{opt}$ $[Wt]$ is the optical power incident on the photodiode, $M$ is a multiplication factor and $G$ is the transimpedance gain of the receiver $[V/Amp]$. Finally, to get $\sigma_n^2$, we get the variance of both sides and so $\sigma_n^2 = \sigma_a^2 M^2 G^2$.

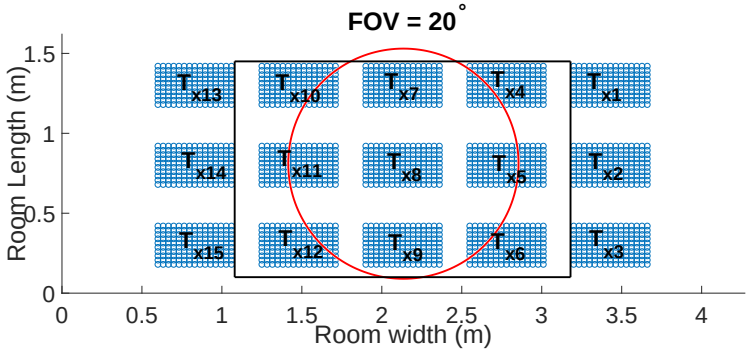


Figure 2: Example of Noise Contributors Impacting a Circular $FOV = 20°$

$$P_n(\chi) = \sum_k \sum_i \frac{P_{txDC}}{wn} \frac{(m+1)A}{2\pi d_{ik}^2} \cos^m \phi_{ik} cos\psi_{ik} 1\{\psi_{ik} \leq \chi\} \tag{6}$$

As for $P_n$ we use Eq. (6), where $P_{txDC}$ is the transmitted DC optical power that contributes to the noise. It is normalized as we divide it by the number of elements in the luminaire grid $wn$. In this calculation we do not need to consider $C_T C_R$ because $P_{txDC}$ is

a number evaluated empirically and encompasses this factor. Note that, the receiver area $A$ is substituted back into the equation to factor the receiver area because $C_T C_R$ is no longer used. All the parameters defined with subscript $i, k$ describe the point source element $i$ within source $k$ that causes noise.

In the noise formula, by changing the FOV $\chi$, we are able to count how many elements are included within the FOV to calculate the total electrical amplitude received at the detector that contributes to shot noise. To clarify, in Fig.2, we can see that if the receiver is in the center of the room and receives its signal from the center transmitter ($T_{x8}$) at 20° FOV then there are 9 sources contributing to the incident noise ($T_{x8}$ included). To calculate the noise we sum the elements from within these 9 transmitters. Therefore, in this instance, $k$ in the FOV is summed from 4 to 12 while $i$ sums up the elements within these transmitters that are in the FOV. Note that we consider non-LOS signals in this configuration to be negligible and do not calculate their impact [14]. Fig.2 also shows the observed range of receiver locations (shown by the black rectangle in the center).

Our goal is to optimize the SNR at the receiver by varying the receiver's FOV. Therefore we form the following optimization problem.

$$\begin{aligned} &\max_{j=1,\ldots,S} && \max_{\chi} \mathsf{SNR}(\chi)_j \\ &\text{s.t.} && \chi_{\min} \leq \chi \leq \chi_{\max} \end{aligned}$$

where $S$ is the total number of transmitters in the room. We define $\chi_{min}$ as the minimum FOV to pick only one transmitter within the FOV and $\chi_{max}$ as the maximum FOV that can cover all the sources in the room when the receiver is flat and facing the lights, both can be deduced geometrically and will be discussed later.

The problem is non-convex and thus we solve the two following problems in their respective order, which together are equivalent to the previous problem, to obtain the best possible FOV for the best SNR that the receiver can achieve within a general room setting.

$$\begin{aligned} &\text{(a)} && \chi_j^* = \arg\max_{\chi} \mathsf{SNR}_j(\chi),\ j = 1, \ldots, S \\ &&& \text{s.t.} \quad \chi_{\min} \leq \chi \leq \chi_{\max} \\ &\text{(b)} && \chi^* = \arg\max_{j=1,\ldots,S} \mathsf{SNR}_j(\chi_j^*) \end{aligned}$$

Problem (a) finds the best FOV for the receiver per transmitter then Problem (b) picks the highest SNR amongst all the transmitters and identifies the FOV $\chi^*$ that yielded this highest SNR.

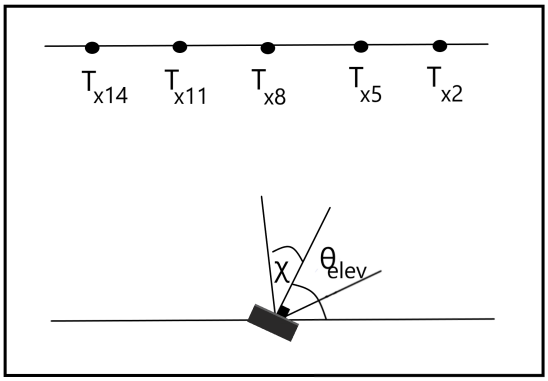


Figure 3: Relationship Between FOV and Elevation for a Mobile Device

Note that device orientation has a significant impact on SNR even when a device is in close proximity to a specific transmitter as its aperture may be pointed away from that transmitter. Using the optimization problem formulated above, we can confirm this by showing results for a receiver centered underneath the transmitter grid. Under $T_{x8}$, for rotations around the x-axis as shown in Fig. 3, we get the best transmitter-FOV pair that give the maximum SNR. We change $\theta_{elev}$ which is the angle between the perpendicular to the receiver and the horizontal plane where the receiver lies, and monitor the output of the problem in terms of transmitter chosen and optimal FOV for maximum SNR reception. The results are shown in Fig. 4. We highlight 5 regions that show the transmitter with highest SNR per each region and the receiver FOV that achieves the highest SNR. Notice that the placement of transmitters in Fig. 3 corresponds to the results seen in Fig. 4. For example, at $\theta_{elev} = 20°$ the transmitter that gives the highest SNR (47 dB) is $T_{x5}$ at FOV $\chi = 58°$. The optimization technique applies information about the physical space including luminaire location, room dimensions, and location and orientation of the receiver, and reveals the FOV and transmitter producing the optimal SNR.

Under receiver mobility, the optimal FOV will be time varying. In this case, there is a need for repeated calculation of the FOV for each change sensed in location or orientation; however, depending on the device speed and the recomputation granularity, it can become impractical to use this approach. For this reason, we propose the algorithm (discussed thoroughly in the following subsection) and distinguish between three possible velocity states: Quasi-Static, Slow, and Fast, since our discussion is mainly concerned with indoor VLC networks.

In the Quasi-Static device scenario; a receiver can solve the optimization mentioned above to get the best FOV ($\chi^*$). On changing its orientation or location the receiver can trigger a recalculation of $\chi^*$. Meanwhile in the Slow velocity scenario, we fix the FOV at some intermediate value $\chi_{med}$ that guarantees connectivity for an untilted device. The intermediate value depends on the size and geometry of the space. If no signals are found due to a tilt in the receiver, the algorithm expands the FOV until at least one transmitter

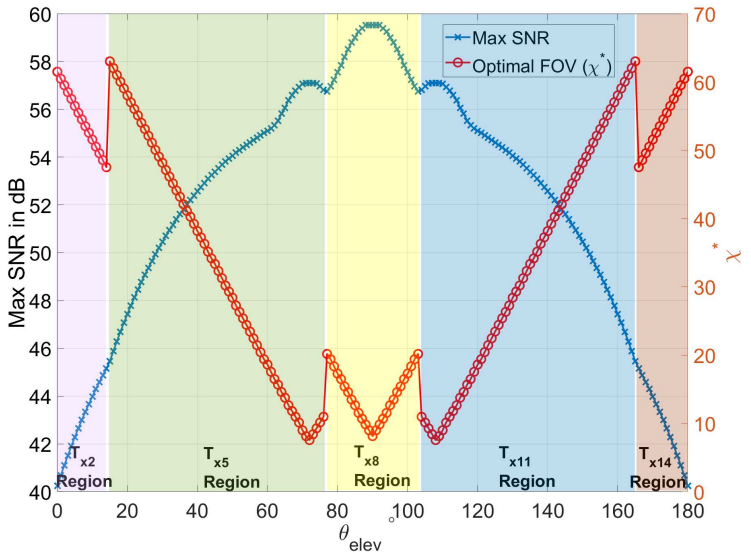


Figure 4: Evaluating the Best (TX-FOV) pair for Optimal SNR at a Receiver Fixed at the Room Center with Variable Orientation

is found. The possible values for $\chi$ in this interval are $\chi_{med} \leq \chi \leq \chi_{max}$.

Finally, for the Fast case (considered in most research to be approximately $2-3$ $m/s$ indoors), we fix $\chi$ at $\chi_{max}$, which is also designed based on the room dimensions to cover all luminaires in the room when the receiver is directed upward from the room center, because the user is moving fast and needs coverage at all times. Note that $\chi_{max}$ is not necessarily 90°.

## 3.2 Velocity and Device Orientation-Based Algorithm

In this section, we introduce the Velocity Orientation Variable FOV (VOV-FOV) algorithm. This algorithm is designed to address practical scenarios in which a fast reaction from the receiver is required to sustain connectivity for mobile users. This algorithm is based on the optimization problem but tunes the FOV differently based on the state of the user velocity.

To study the impact of device velocity, we model device motion as a random walk with $N$ steps and model velocity in a block-fading-model fashion, where velocity is fixed over a number of blocks $N_b$. The device's elevation angle is uniformly variable between an interval of 0° and 15° and its azimuth angle is fixed at 0°. The user's velocity can be in one of three possible intervals (states): quasi-static, slow or fast. This yields two thresholds between these intervals. We also introduce and define the concept of a *coverage hole* as any location in the physical space where the receiver receives no signal from any of the available transmitters.

VOV-FOV Algorithm

**Input:** Number of steps N, Block length $N_b$, $\{V_1, \ldots, V_N\}$
Initialization: Set Room dimensions, number of sources and their positions, receiver info.
**for** n=1:N **do**
    Calculate Fixed FOV SNR: $\max_j \mathsf{SNR_j}(90)$ from eqn. (4)
    **if** $V_n > V_{T2}$ (Fast State) **then**
        $\chi = \chi_{\max}$
        Calculate $\mathsf{SNR_j}(\chi)$ from eqn. (4)
    **else if** $V_n < V_{T1}$ (Quasi-Static State) **then**
        Calculate $\mathsf{SNR}_j(\chi), \forall j$ from eqn. (4)
        **if** $\max_j \mathsf{SNR}_j(\chi) = 0$ **then**
            **while** $\max_j \mathsf{SNR}_j(\chi) = 0$ and $\chi < \chi_{\max}$ **do**
                $\chi = \chi + \chi_{\text{step}}$
                Calculate $\mathsf{SNR}_{j,+}(\chi) \triangleq \mathsf{SNR}_j(\chi + \chi_{\text{step}})$
                **if** $\max_j \mathsf{SNR}_{j,+}(\chi) < \max_j \mathsf{SNR}_j(\chi)$ **then**
                    break;
                **end if**
            **end while**
        **else**
            Calculate $\mathsf{SNR}_{j,-}(\chi) \triangleq \mathsf{SNR}_j(\chi - \chi_{\text{step}})$, $\forall j$ and $\mathsf{SNR}_{j,+}(\chi)$ $\forall j$
            **if** $\max_j \mathsf{SNR}_{j,+}(\chi) > \max_j \mathsf{SNR}_{j,-}(\chi)$ **then**
                Keep Increasing $\chi$ till $\chi_{\max}$ or $\max_j \mathsf{SNR}_{j,+}(\chi) < \max_j \mathsf{SNR}_{j,-}(\chi)$.
            **else**
                Keep Decreasing $\chi$ till $\chi_{\min}$ or $\max_j \mathsf{SNR}_{j,+}(\chi) > \max_j \mathsf{SNR}_{j,-}(\chi)$.
            **end if**
        **end if**
    **else**(Slow State)
        $\chi = \chi_{\text{med}}$
        Calculate $\mathsf{SNR}_j(\chi), \forall j$
        **if** $\max_j \mathsf{SNR}_j(\chi) = 0$ **then**
            Increase $\chi$ until $\exists j$ s.t. $\mathsf{SNR}_j(\chi) \neq 0$ while $\chi < \chi_{\max}$
        **end if**
    **end if**
**end for**
Calculate Average max Variable FOV SNR Vs. Average max Fixed FOV SNR

The algorithm decides in which category the user velocity lies, and then initiates different actions based on each category, described below.

- **Quasi-Static interval:** If a user velocity is below the first threshold $V_{T1}$, it is considered quasi-static and, based on device orientation changes, the receiver FOV is reduced/increased gradually in steps ,$\chi_{step}$, until the best SNR is reached. FOV reaches the minimum $\chi_{min}$ if the device is untilted and is directly under the transmitter.

Otherwise the best SNR is reached through tuning by the algorithm. $\chi_{min}$ is designed to only show 1 transmitter in the receiver FOV, considering a circular transmitter and based on knowing its radius $R$ and height $L$ away from the receiver plane. This can be calculated as $\chi_{min} = \tan^{-1} \frac{R}{L}$.

- **Slow interval:** In this case, the user velocity is between the two thresholds $V_{T1}$ and $V_{T2}$. The device is considered moving slowly in which case having a variable FOV still allows for improvement in SNR but still needs a faster response from the receiver because the device is already on the move. This is why as soon as the velocity is in this range, the algorithm sets the FOV to a medium FOV, $\chi_{med}$. In our lab scenario, $\chi_{med}$ is established by setting the receiver FOV with a view of 4 transmitters when centered between them and directed upward. However, under different room conditions (e.g., less dense scenario), then perhaps 2 transmitters in view may be more appropriate. The algorithm then checks to see if the receiver is trapped in a coverage hole due to $\chi_{med}$. If so, it gradually increases the FOV to locate an available signal to escape the coverage hole. The algorithm re-evaluates when location, velocity or orientation change.

- **Fast interval:** This is when the user velocity is above a threshold $V_{T2}$. In this case, a wide FOV is preferred that covers all the transmitters and minimizes dropouts. For this case we fix the FOV at $\chi_{max}$. Note that, $\chi_{max}$ does not necessarily need to be a maximal value (e.g., 90°). Recall that the maximum FOV also attracts a higher noise floor and thus the smallest FOV that can cover all the transmitters is desirable. Fig. 6 shows the impact of fixing the FOV to be less than $\chi_{max}$ and, in the fast state, how this choice can provide a higher average maximum SNR but also introduce coverage holes. This tradeoff is discussed in more detail in Section 4.

The VOV-FOV algorithm dynamically tunes the receiver FOV to obtain the highest SNR for a receiver given the orientation and the location of the device whether it is static or moving. The different operating procedures per velocity interval allow it to be flexible so that user receiver does not suffer from coverage holes or low signal quality especially when mobile. The step size of the algorithm (how much the FOV changes on an iteration) impacts the instantaneous difference between the FOV and the optimal value. Different step sizes are interesting especially because the circular view area is quadratic in FOV step size. Fig. 5 shows how the number of transmitter elements found in range is linked to FOV step size expansion for a fixed room size. The figure shows the growth of FOV when the receiver is centered in the room. Once all elements are in the FOV ($\chi_{max}$ is reached), the cumulative effect of the visible APs reaches its limit. There is also an inherent tradeoff between step size and the convergence time for the algorithm; i.e., the smaller the step size, the longer it takes to converge to the solution, yet the closer the result is to the optimal. Thus step size should be tuned according to room design and the accuracy expected from the receiver.

While the algorithm in the quasi-static interval resembles the gradient descent method [15], it differs in that it moves in the direction opposite to the gradient but not taking into account the actual gradient value within the step. This is mainly because we choose to fix the step to produce faster results to the receiver.

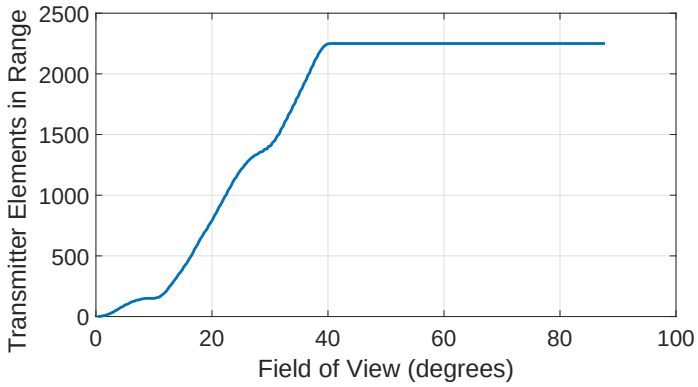


Figure 5: Number of Transmitter Elements Seen by the Receiver in Expanding FOV

# 4 Analysis and Simulation Results

In this section we show predicted performance results based on the proposed D-FOV technique, the system models, and the VOV-FOV Algorithm. Whereas the simulated results relate to our testbed configuration, the models are generally applicable to any instance of an indoor AP configuration. Our results are based on the study of different sets of APs including cases for 3, 6, 9, and 15 APs (corresponding to the testbed). The simulation parameters for the algorithm are summarized in Table 1.

The results from VOV-FOV Algorithm confirm the benefits of dynamically changing the FOV to achieve higher SNR. The results also highlight the need to balance the number of sources within a room, how they are spaced, and the inherent trade-off between coverage and SNR. Tradeoffs are possible to yield higher SNR if one is willing to sacrifice continuous connectivity and vice-versa. Through optimization it is possible to find the FOV that provides satisfactory performance in both continuity and SNR.

While we care about maintaining the best coverage in the quasi-static and slow cases by dynamically changing the FOV to tune it to the best SNR, we need to fix the FOV in the fast scenario, mainly because the user's speed will not allow for useful optimization in the limited time available to traverse the room. During the transit time the optimal FOV may have changed before a new computation is complete. Note also that the sensitivity of the receiver to orientation increases with the decrease in FOV.

We evaluated three different fixed FOVs for the same random walk pattern for the fast case as shown in Fig. 6. This includes $\chi_{max}$, which yields full coverage but the least average maximum SNR, 108, $\chi_{med} = 27°$ which ensures that a flat receiver is always covered by 2 transmitters when we simulate between the possible number of sources (for a less dense network). The latter achieves 99.24% coverage in the shown scenario but allows for a higher maximum SNR on average than $\chi_{max}$, with coverage holes only in the room corners that are tolerable in most cases. Finally $\chi_{med} = 17°$ ensures being covered by 4 transmitters (useful in more dense optical networks) and gives the best SNR performance on average but produces more coverage holes at 96.18% coverage of the random walk. Note that these results are from

Table 1: Simulation Parameters

| Parameter | Parameter Description | Value |
|---|---|---|
| $m$ | Lambertian order | 0.88 |
| B | Bandwidth | $5 \times 10^7$ Hz |
| A | Receiver area | $785 \times 10^{-9}$ $m^2$ |
| $V_{T1}$ | Velocity threshold 1 | 0.1 $m/s$ |
| $V_{T2}$ | Velocity threshold 2 | 0.5 $m/s$ |
| $\chi_{min}$ | Minimum FOV | 7° |
| $\chi_{med1}$ | Medium FOV 1 | 17° |
| $\chi_{med2}$ | Medium FOV 2 | 27° |
| $\chi_{step}$ | FOV step | 7° |
| $\chi_{max}$ | Maximum FOV | 40° |
| $C_T C_R$ | Constants @100$kHz$ | 1.4 |
| $N_b$ | Blocks | 5 |
| $N$ | Random walk steps | $5,000$ |
| $A_{tx}$ | Transmitted amplitude | 1.4 pk-pk |
| S | Number of sources | 3,6,9,15 |
| $w$ | $T_x$ Element grid width | 15 |
| $n$ | $T_x$ Element grid length | 10 |
| $R$ | Responsivity | 28 |
| $M$ | Multiplication factor | 57 |
| $G$ | Transimpedance gain | $10^5$ $V/A$ |
| $i_d^2$ | Dark current noise | $68 \times 10^{-20}$ $A^2$ |
| $P_{txDC}$ | Noise DC power | 0.0022 $V$ |

the variable FOV algorithm and we only fix the FOV in the Fast case. This same scenario gives full coverage in the fixed FOV baseline and an average maximum SNR of 35.

Figs. 7 and 8 show the tradeoffs discussed but for different number of sources vs. the baseline fixed FOV of 90° adopted by most works. Both our baseline and novel algorithms consider orientation and location with the added advantage of including velocity as a parameter. This addition specifically improves results in our lab setting almost three times (3X) better than the baseline fixed FOV case. We argue that the higher the noise in an environment the better our algorithm will perform because it will be able to mask more noise than the case of lower noise setting. Fig. 7 shows the improvement in average max SNR in the 3 cases of fixed fast FOV mentioned above versus the baseline fixed FOV meanwhile Fig. 8 shows how the improvement between the 3 variable FOV cases arises and shows the coverage loss percentage for each of these cases versus number of sources. The scenario at 15 sources in both of these figures is shown in detail in Fig. 6.

Each of Figs. 7 and 8 shows how having a dense network improves coverage and average maximum SNR. Note however, a dense network providing multiple access must also reconcile frequency assignment or other means to mitigate inter-cell SINR, which is beyond the scope of this paper.

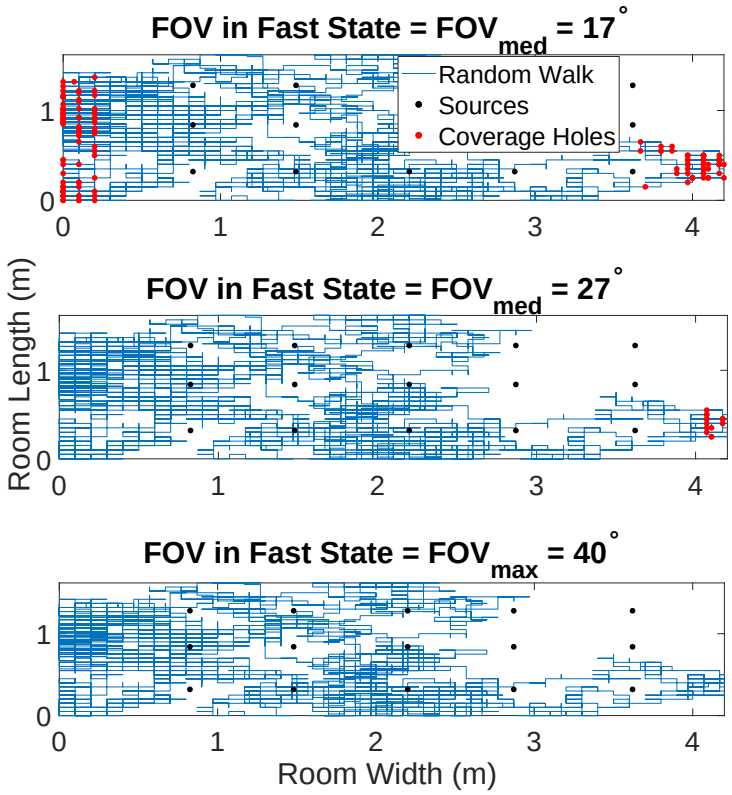


Figure 6: Coverage Holes for Different Fixed FOVs in the Fast State: For FOV = 17°, Average Max SNR = 170.9. While for FOV = 27°, Average Max SNR = 118.4 and for FOV = 40°, Average Max SNR = 108.

# 5 Experiments and Results

Here we describe the testbed environment and show results of experimentation with D-FOV receiver under a full range of angular and aperture control.

## 5.1 Testbed Configuration

Our testbed at Boston University (Fig. 9) is comprised of a $3 \times 5$ grid of off-the-shelf CREE luminaires (#CR22-32L-35K-S) with dimensions of 46 $cm \times 24$ $cm$. The grid dimensions are 427 $cm \times 162$ $cm$ $(x \times y)$. This layout corresponds the dimensions shown earlier in Fig. 2.

The luminaires are positioned from the center in increments of 0.7 $m$ in the x-axis and 0.5 $m$ in the y-axis at a height of 2.68 $m$ from the floor. The luminaires each transmit a unique frequency assigned in the range of 100 kHz to 800 kHz in 50 kHz increments. The height between the luminaires and the receiver plane is 1.96 $m$.

We use an avalanche photodiode (ThorLabs unit (#APD120A2)) as the receiver mounted on a custom turret that can pan (rotate), vary its aperture, and tilt, hence the name PATT.

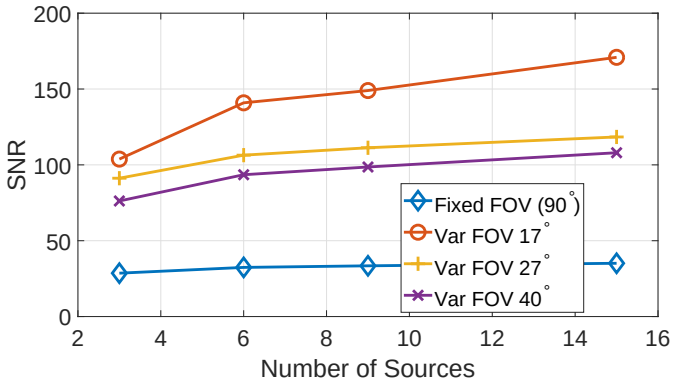


Figure 7: Average Maximum SNR for Different FOVs vs. Number of Transmitters

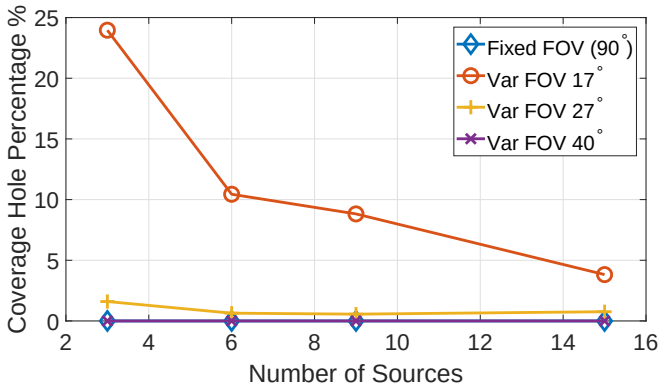


Figure 8: Percentage of Coverage Holes for Different FOVs vs. Number of Transmitters

The aperture is manipulated using a circular mechanical iris (Thorlabs #ID50/M). The turret and the x-y translational unit are each directed by a micro-controller interfaced to a central control station. The control station is programmed to move the turret position and velocity based on the sequencing defined for our experiments.

The receiver is connected to an N210 USRP attached to an additional computer running Gnu Radio software and is automated to collect measured data. The signal chain involves driving each luminiare using one of the 15 USRP channels with unique frequency, conversion of electrical to optical by each luminiaire, conversion of optical to electrical at the receiver, and then finally calculating the electrical power corresponding to each received sinusoid. This last step is achieved through an FFT operation using the USRP/Gnu Radio [16] framework, producing the peak-to-peak voltage of the received sinusoids and then the peak-to-peak optical power (as in the numerator calculation of Eq. 2).

We directly relate the received optical power to the received amplitude as optical power is directly proportional to current in the optical domain. (Note: the CREE luminaires have a limited frequency response that is apparent within the set of test frequencies used to identify each transmitter, but is not germane to the experiments. In practice each transmitter will exploit the full viable frequency range of the luminaire used.)

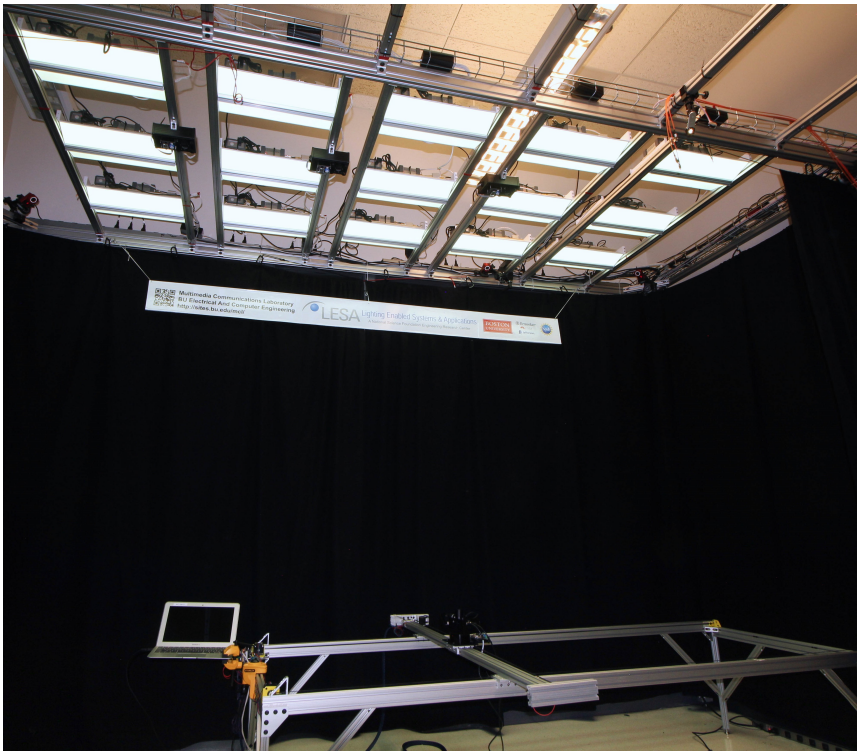


Figure 9: Dense VLC Testbed at Boston University

The turret and platform are sequenced to collect data in a grid by ranging over 12 points in the x-axis and 7 points in the y-axis. At each coordinate 9 different FOVs are evaluated, each at 2 tilt angles. In this data set, we fix the receiver azimuth angle to zero.

## 5.2 Experimental Results from Testbed

Data are collected under different operating conditions in the testbed to show the impact of tilt, position on the grid, and FOV.

We show 4 experimental runs: 1. Measuring Received Signal Strength (RSS) from one transmitter for different FOVs for an untilted circular aperture receiver. 2. Measuring RSS from one transmitter for different FOVs for a circular aperture receiver with $\theta_{elev} = 120°$. 3. Measuring RSS from all transmitters for a fixed FOV for an untilted circular aperture receiver. 4. Measuring RSS from one transmitter for different FOVs for an untilted non-circular aperture receiver.

Recall that the transmitters are arranged as shown in Fig. 2 with a collection area corresponding to the center rectangle. We show and discuss results for the transmitter in the center of the grid, $T_{x8}$.

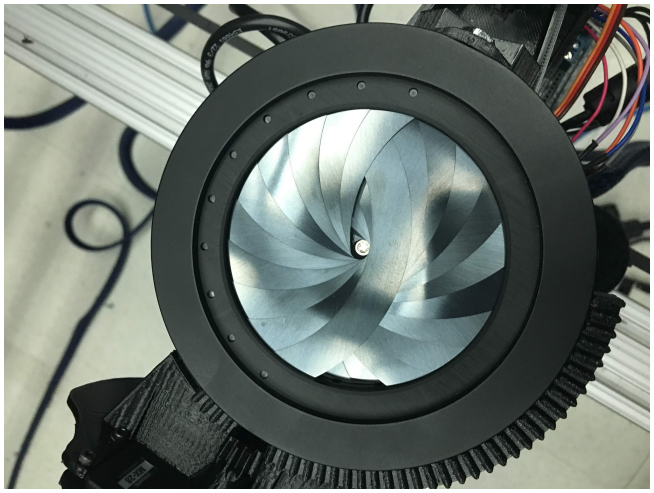

(a) Variable FOV Receiver (Partially Oval Aperture)

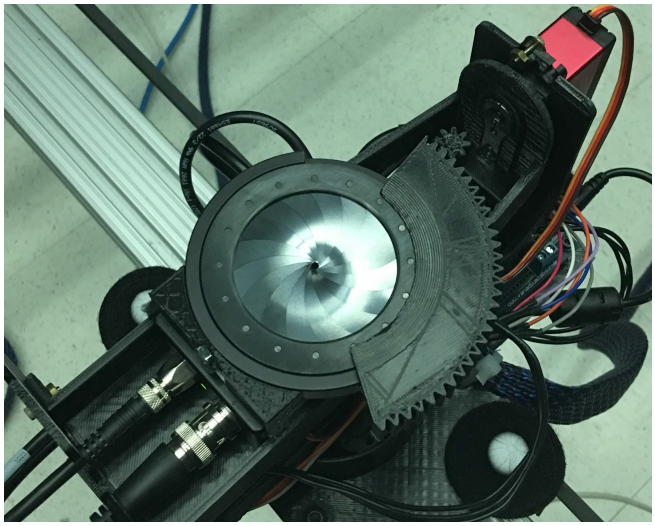

(b) Variable FOV Receiver (Circular Aperture)

Figure 10: Receiver Detail for Partially Oval and Circular Aperture Turrets

### 5.2.1 Using a Circular FOV

Fig. 11(a) shows the effect of the variable FOV on the receiver SNR using the circular aperture iris (Fig. 10 (b)). The figure shows each SNR value received from $T_{x8}$ under 9 FOVs ranging from 7.1° to 72.3°. The curve illustrates the SNR-coverage tradeoff: when the receiver is directly below the center transmitter, it can either narrow the FOV to improve SNR, or enlarge the FOV to maximize coverage. This tradeoff guides the optimization for each receiver position and orientation.

Meanwhile, Fig. 11(b) shows the impact of receiver tilt on the received signal from transmitter 8 at $\theta_{elev} = 120°$ using the circular aperture iris (Fig. 10 (b)). This plot shows why orientation has an important role in determining the optimal FOV for the given receiver location, position, and velocity. In this example, the configuration leads to a low SNR when

the receiver is directly under transmitter 8 but tilted. A better signal under transmitter 8 is obtained by a connection to transmitter 11 in the case of Fig. 12. This shows the SNR received from transmitter 11 at the same 120° tilt. This result also agrees with the optimization shown in Fig. 4.

Figures 13(a) and 13(b) show the SNR received from each transmitter in the middle section of the lab (transmitters $4-12$) at maximum and minimum FOV respectively, while the receiver is untilted. For each case, a smaller FOV realizes a more concentrated signal, with fewer noise sources, but also creates more coverage holes. The maximum FOV scenario shows signal continuity with a sacrifice in the SNR in comparison to the minimum FOV scenario.

As mentioned earlier, the CREE luminaires have a frequency-dependent signal attenuation that disadvantages higher frequencies. Due to the range of test frequencies used to isolate individual luminaires, there is a pattern of signal strength attributed to this frequency selection that is apparent in Fig. 13 but is only an artifact of the limits of the luminaires used in the testbed.

Fig. 14 shows the maximum SNR calculated using theoretical noise vs. noise measured in the lab. The figure reveals that the noise model provides a reasonable approximation of the lab environment. However, we expect, and it has been our experience, that minimizing noise in the lab instrumentation requires careful attention to detail. The development of practical VLC systems will certainly need to be robust to these practical considerations.

Although not shown here, prior work indicates that the measured results also conform well with the model simulation [9] in spite of the point source assumption for the rectangular "troffer" luminaires.

Fig. 14 also shows that for the two theoretical curves, allowing the FOV to be a continuous set provides smoother results than when it is restricted to the FOVs given to the receiver algorithm, of course this also depends on the FOV step chosen as discussed in Section 3.

### 5.2.2 Using Different FOV Shape

The results above consider a receiver with circular aperture consistent with the fabrication of optical components such as lenses, lens tubes, and irises. However, photodetectors are often rectangular, as are the arrays of luminaires deployed as lighting. There are perhaps alternative geometries that support maximizing performance in an adaptive receiver design matching the receiver perspective to the transmitter layout.

For example, a different aperture shape might realize a different coverage region and a different set of coverage holes. Although not a complete investigation of possible FOV shapes, we explore the impact of using a non uniformly circular aperture (Thorlabs #ID75Z), which is oval in smaller FOVs and then conforms to the circular FOV at larger FOVs. Fig. 15 shows SNR for the partially oval aperture at different FOVs when the receiver is flat and

positioned under transmitter 8.

We notice that at the minimum FOV, while the circular iris shows only one signal, the non-uniform iris shows two and with the increase in FOV it adds more signals faster than the circular iris while still allowing less noise to enter than the wide FOV aperture but more than the circular aperture noise. This behavior is potentially valuable in a scenario where diversity is needed at a lower noise floor than what the wide FOV provides. This result motivates us to explore the interaction among diversity, interference, the shapes of the receiver, aperture, and lighting array in future works.

The two turrets used in the experiments are shown in Fig. 10.

Fig. 10(a) shows the partially oval aperture iris (Thorlabs #ID75Z) while Fig. 10(b) shows the circular aperture iris (Thorlabs #ID50/M).

## 5.3 Other Considerations

There are additional considerations for the performance of VLC receivers that we encountered during this study that warrant additional exploration. These include the use of lenses and other optical components, the impact of different room designs and dimensions, and the responsiveness of the aperture control.

With respect to the FOV manipulation, we chose to use a mechanical iris mounted above the plane of the receiver sensor surface, controlling the angle of signal arrival at the receiver. The FOV can also be manipulated or enhanced using lenses or other optical components which can be bulky or more complex to control. Ultimately the ideal receiver design will utilize a combination of optical elements that realize the required range of control and fit within the size and cost constraints for the application.

The dimensions and placement of luminaires in the physical space is also important. Lights can be deployed for lighting function and/or aesthetics, but deployment is often compromised under cost or construction constraints and without strict illumination guidelines. Clearly there is an opportunity to factor in lighting deployment to improve coverage as optical APs, but reconciling practical lighting design and placement is beyond the scope of this paper.

Finally, the control of the FOV requires responsiveness comparable to the dynamics of the receiver motion. Although human-scale mobility is relatively slow, device orientation (angle) changes can be quite fast and are amplified by the distance to the transmitters. For the D-FOV receiver to be successful, it must have sufficient performance matched to the orientation dynamics in order to sustain continuous link connections, minimize coverage holes, and sustain high SNR.

# 6 Conclusion and Future Work

In this paper we propose D-FOV receiver and the corresponding VOV-FOV algorithm intended to adapt to the velocity, position, and orientation of a mobile device in a dense VLC indoor network. The results, supported by analysis, simulation, and experimentation, show the potential to greatly enhance performance for VLC links by manipulating the FOV of a receiver. The work demonstrates promise for implementation of novel receiver architectures that are able to compensate for device dynamics under mobility. Finally, because D-FOV controls the amount of interference from neighboring transmitters, there is an opportunity to apply our technique to increase area spectral efficiency and thus overall system performance in dense optical systems. We plan to study this impact in future work.

# Acknowledgement

This work was supported in part by the Engineering Research Centers Program of the National Science Foundation under NSF Cooperative Agreement No. EEC-0812056 and by NSF No. CNS-1617924. The authors thank Constantinos Gerontis for helping design, build, and collect data with PATT, and Emily Lam for the design and build of MATT. The authors also thank Islam El Bakoury for his helpful discussions and valuable input.

# References

[1] Karunatilaka, D., Zafar, F., Kalavally, V., Parthiban, R.: 'LED based indoor visible light communications: state of the art,' *IEEE Commun. Surveys Tut.*, Q3 2015, **17**, (3), pp. 1649–1678.

[2] Pathak, P.H, Feng, X., Hu, P., Mohapatra, P.: 'Visible light communication, networking, and sensing: a survey, potential and challenges,' *IEEE Commun. Surveys Tut.*, Q4 2015, **17**, (4), pp. 2047–2077.

[3] Rahaim, M.B., Morrison, J., Little, T.D.C.: 'Beam control for indoor FSO and dynamic dual-use VLC lighting systems,' *J. Comm. and Info. Networks*, December 2017, **2**, (4), pp. 11–27 Available: https://doi.org/10.1007/s41650-017-0041-7.

[4] Rahaim, M.B., Little, T.D.C.: 'Toward practical integration of dual-use VLC within 5G networks,' *IEEE Wireless Comm.*, August 2015, **22**, (4), pp. 97–103.

[5] Elgala, H., Mesleh, R., Haas, H.: 'Indoor optical wireless communication: potential and state-of-the-art,' *IEEE Commun. Mag.*, September 2011, **49**, (9), pp. 56–62.

[6] Vavoulas, A., Sandalidis, H.G., Tsiftsis, T.A., Vaiopoulos, N.: 'Coverage aspects of indoor VLC networks,' *J. Lightwave Technol.*, December 2015, **33**, (23), pp. 4915–4921. Available: http://jlt.osa.org/abstract.cfm?URI=jlt-33-23-4915

[7] Liu, J., Li, Q., Zhang, X.: 'Cellular coverage optimization for indoor visible light communication and illumination networks,' *J. Comm.*, November 2014, **9**, (11), pp. 891–898.

[8] Bas, C.L., Sahuguede, S., Julien-Vergonjanne, A., Behlouli, A., Combeau, P., Aveneau, L.: 'Impact of receiver orientation and position on visible light communication link performance,' *Proc. 4th Intl. Workshop on Opt. Wireless Comm. (IWOW)*, Istanbul, Turkey, September 2015, pp. 1–5.

[9] Abdalla, I., Rahaim, M.B., Little, T.D.C.: 'Impact of receiver FOV and orientation on dense optical networks', *Proc. IEEE Globecom*, Abu Dhabi, UAE, December 2018.

[10] Little, T.D.C., Rahaim, M.B., Abdalla, I., Lam, E.W., Mcallister, R., Vegni, A.M.: 'A multi-cell lighting testbed for VLC and VLP,' *Proc. Global LIFI Congress*, Paris, France, February 2018, pp. 1–6.

[11] Kahn, J.M., Barry ,J.R.: 'Wireless infrared communications,' *Proc. IEEE*, February 1997, **85**, (2), pp. 265–298.

[12] 'Thorlabs apd110x/120x Operation Manual 2013,' https://www.thorlabs.com/, accessed August 2018.

[13] Ramirez-Iniguez, R., Idrus, S., Sun, Z.: 'Optical wireless communications' (Auerbach Publications, New York, 2008).

[14] Komine, T., Nakagawa, M.: 'Fundamental analysis for visible-light communication system using LED lights,' *IEEE Trans. Consum. Electron.*, February 2004, **50**, (1), pp. 100–107.

[15] Bertsimas, D., Tsitsiklis, J.: 'Introduction to linear optimization' (Athena Scientific, 1997).

[16] 'GNU Radio software,' https://gnuradio.org/, accessed May 2018.

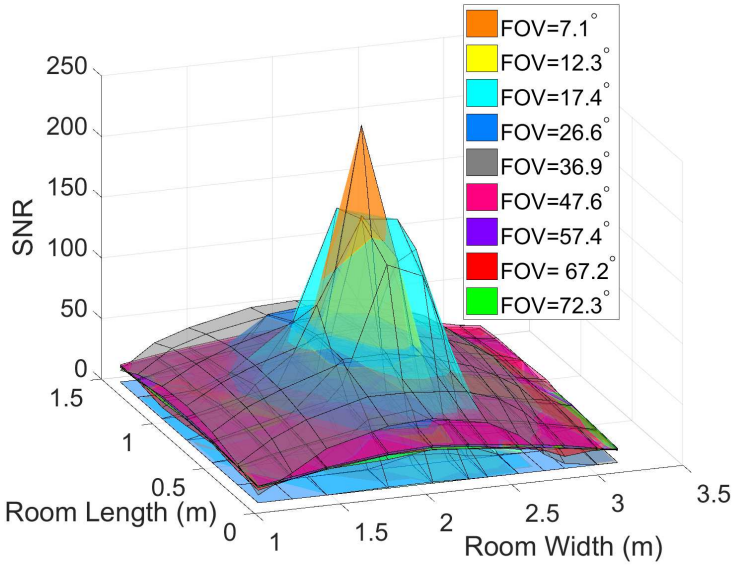


(a) SNR under $T_{x8}$ for a Flat Circular Aperture Receiver at Different FOVs

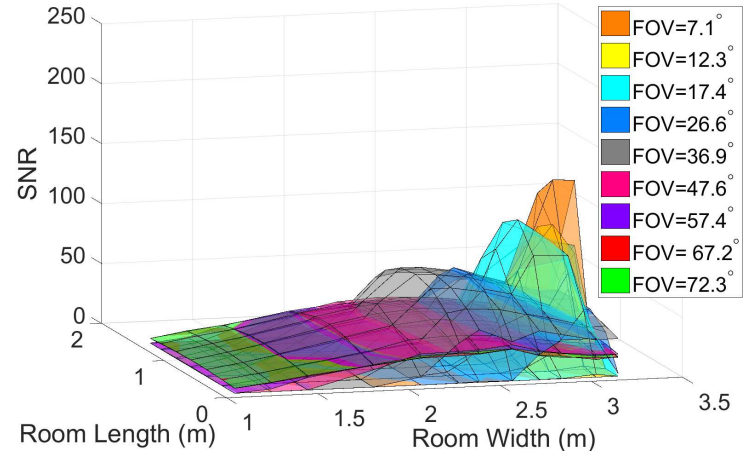


(b) SNR under $T_{x8}$ for a $\theta_{elev} = 120°$ Tilted Circular Aperture Receiver at Different FOVs

Figure 11: SNR under $T_{x8}$ for a Flat Circular Aperture Receiver vs. a $\theta_{elev} = 120°$ Tilted Circular Aperture Receiver at Different FOVs

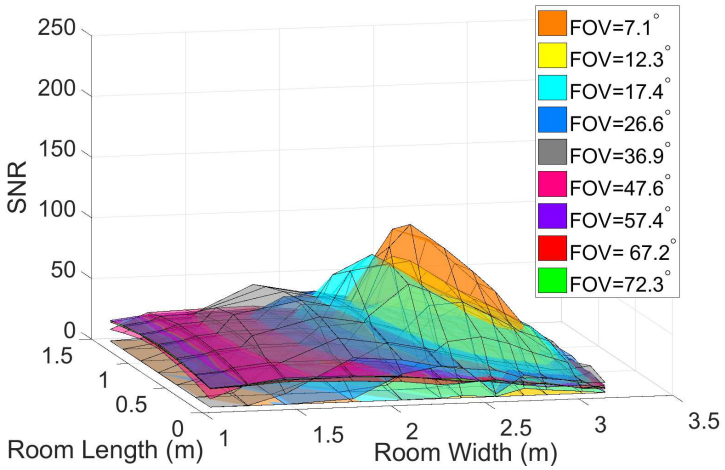


Figure 12: SNR Under $T_{x11}$ for a $\theta_{elev} = 120°$ Tilted Circular Aperture Receiver at Different FOVs

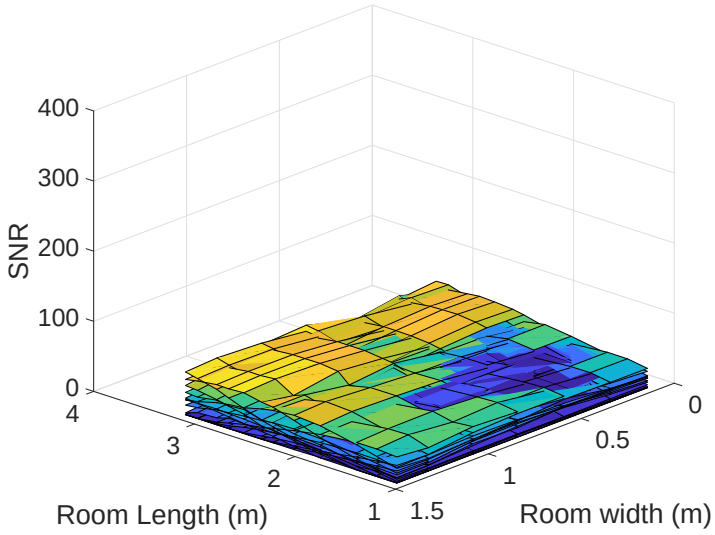


(a) SNR Under All Transmitters for a Flat Facing Upwards Circular Aperture Receiver at Maximum FOV (40.1°)

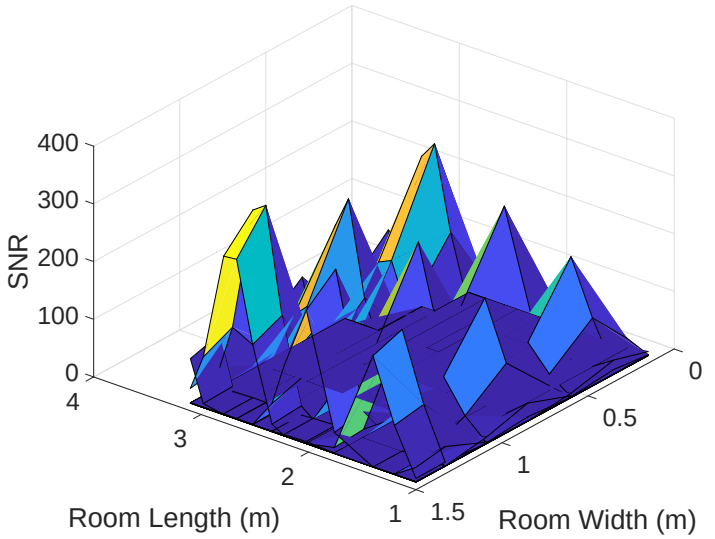


(b) SNR Under All Transmitters for a Flat Circular Aperture Receiver at Minimum FOV (7.1°)

Figure 13: SNR Under All Transmitters for a Flat Circular Aperture Receiver at $\chi_{min}$ vs $\chi_{max}$

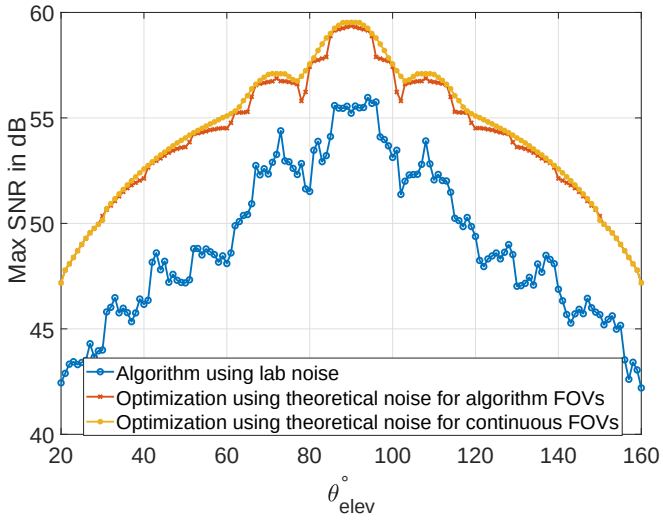


Figure 14: Maximum SNR Calculated Through Theoretical Noise Model vs. Measured Lab Noise

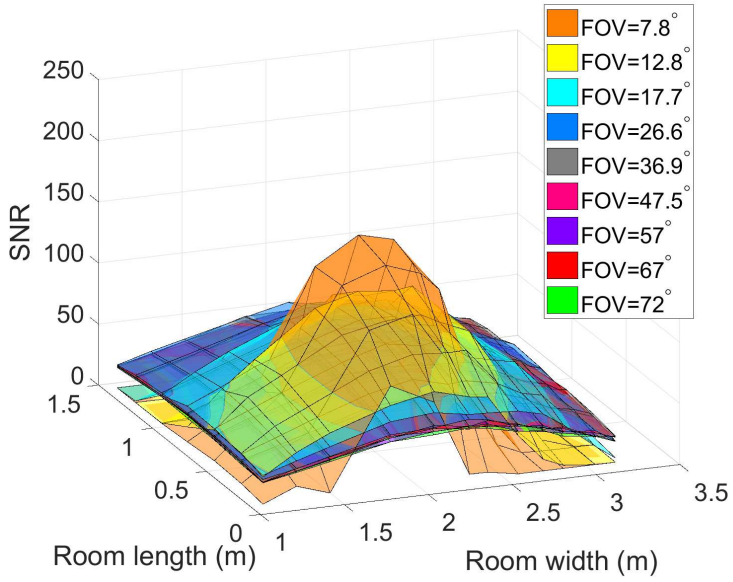


Figure 15: SNR under $T_{x8}$ for a Flat Partially Oval Aperture Receiver at Different FOVs